

L.; Zhang, S. Q.; Zhang, X. Y.; Zhang, Y.; Zhang, Y.; Zhang, Y. H.; Zhang, Y. N.; Zhang, Y. T.; Zhang, Yu; Zhang, Z. H.; Zhang, Z. P.; Zhang, Z. Y.; Zhao, G.; Zhao, J. W.; Zhao, J. Y.; Zhao, J. Z.; Zhao, Lei; Zhao, Ling; Zhao, M. G.; Zhao, Q.; Zhao, Q. W.; Zhao, S. J.; Zhao, T. C.; Zhao, Y. B.; Zhao, Z. G.; Zhemchugov, A.; Zheng, B.; Zheng, J. P.; Zheng, W. J.; Zheng, Y. H.; Zhong, B.; Zhou, L.; Zhou, X.; Zhou, X. K.; Zhou, X. R.; Zhou, X. Y.; Zhu, K.; Zhu, K. J.; Zhu, S.; Zhu, S. H.; Zhu, X. L.; Zhu, Y. C.; Zhu, Y. S.; Zhu, Z. A.; Zhuang, J.; Zotti, L.; Zou, B. S.; Zou, J. H.. - In: PHYSICS LETTERS. SECTION B. - ISSN 0370-2693. - 770:(2017), pp. 217-225. [10.1016/j.physletb.2017.04.048]

Study of J/ψ and $\psi(3686) \rightarrow \Sigma(1385)^0 \bar{\Sigma}(1385)^0$ and $\Xi^0 \bar{\Xi}^0$

M. Ablikim¹, M. N. Achasov^{9,e}, S. Ahmed¹⁴, X. C. Ai¹, O. Albayrak⁵, M. Albrecht⁴, D. J. Ambrose⁴⁴, A. Amoroso^{49A,49C}, F. F. An¹, Q. An^{46,a}, J. Z. Bai¹, O. Bakina²³, R. Baldini Ferroli^{20A}, Y. Ban³¹, D. W. Bennett¹⁹, J. V. Bennett⁵, N. Berger²², M. Bertani^{20A}, D. Bettoni^{21A}, J. M. Bian⁴³, F. Bianchi^{49A,49C}, E. Boger^{23,c}, I. Boyko²³, R. A. Briere⁵, H. Cai⁵¹, X. Cai^{1,a}, O. Cakir^{40A}, A. Calcaterra^{20A}, G. F. Cao¹, S. A. Cetin^{40B}, J. Chai^{49C}, J. F. Chang^{1,a}, G. Chelkov^{23,c,d}, G. Chen¹, H. S. Chen¹, J. C. Chen¹, M. L. Chen^{1,a}, S. Chen⁴¹, S. J. Chen²⁹, X. Chen^{1,a}, X. R. Chen²⁶, Y. B. Chen^{1,a}, X. K. Chu³¹, G. Cibinetto^{21A}, H. L. Dai^{1,a}, J. P. Dai^{34,j}, A. Dbeysy¹⁴, D. Dedovich²³, Z. Y. Deng¹, A. Denig²², I. Denysenko²³, M. Destefanis^{49A,49C}, F. De Mori^{49A,49C}, Y. Ding²⁷, C. Dong³⁰, J. Dong^{1,a}, L. Y. Dong¹, M. Y. Dong^{1,a}, Z. L. Dou²⁹, S. X. Du⁵³, P. F. Duan¹, J. Z. Fan³⁹, J. Fang^{1,a}, S. S. Fang¹, X. Fang^{46,a}, Y. Fang¹, R. Farinelli^{21A,21B}, L. Fava^{49B,49C}, F. Feldbauer²², G. Felici^{20A}, C. Q. Feng^{46,a}, E. Fioravanti^{21A}, M. Fritsch^{14,22}, C. D. Fu¹, Q. Gao¹, X. L. Gao^{46,a}, Y. Gao³⁹, Z. Gao^{46,a}, I. Garzia^{21A}, K. Goetzen¹⁰, L. Gong³⁰, W. X. Gong^{1,a}, W. Gradl²², M. Greco^{49A,49C}, M. H. Gu^{1,a}, Y. T. Gu¹², Y. H. Guan¹, A. Q. Guo¹, L. B. Guo²⁸, R. P. Guo¹, Y. Guo¹, Y. P. Guo²², Z. Haddadi²⁵, A. Hafner²², S. Han⁵¹, X. Q. Hao¹⁵, F. A. Harris⁴², K. L. He¹, F. H. Heinsius⁴, T. Held⁴, Y. K. Heng^{1,a}, T. Holtmann⁴, Z. L. Hou¹, C. Hu²⁸, H. M. Hu¹, T. Hu^{1,a}, Y. Hu¹, G. S. Huang^{46,a}, J. S. Huang¹⁵, X. T. Huang³³, X. Z. Huang²⁹, Z. L. Huang²⁷, T. Hussain⁴⁸, W. Ikegami Andersson⁵⁰, Q. Ji¹, Q. P. Ji¹⁵, X. B. Ji¹, X. L. Ji^{1,a}, L. W. Jiang⁵¹, X. S. Jiang^{1,a}, X. Y. Jiang³⁰, J. B. Jiao³³, Z. Jiao¹⁷, D. P. Jin^{1,a}, S. Jin¹, T. Johansson⁵⁰, A. Julin⁴³, N. Kalantar-Nayestanaki²⁵, X. L. Kang¹, X. S. Kang³⁰, M. Kavatsyuk²⁵, B. C. Ke⁵, P. Kiese²², R. Kliemt¹⁰, B. Kloss²², O. B. Kolcu^{40B,h}, B. Kopf⁴, M. Kornicer⁴², A. Kupsc⁵⁰, W. Kühn²⁴, J. S. Lange²⁴, M. Lara¹⁹, P. Larin¹⁴, H. Leithoff²², C. Leng^{49C}, C. Li⁵⁰, Cheng Li^{46,a}, D. M. Li⁵³, F. Li^{1,a}, F. Y. Li³¹, G. Li¹, H. B. Li¹, H. J. Li¹, J. C. Li¹, Jin Li³², K. Li¹³, K. Li³³, Lei Li³, P. R. Li^{7,41}, Q. Y. Li³³, T. Li³³, W. D. Li¹, W. G. Li¹, X. L. Li³³, X. N. Li^{1,a}, X. Q. Li³⁰, Y. B. Li², Z. B. Li³⁸, H. Liang^{46,a}, Y. F. Liang³⁶, Y. T. Liang²⁴, G. R. Liao¹¹, D. X. Lin¹⁴, B. Liu^{34,j}, B. J. Liu¹, C. X. Liu¹, D. Liu^{46,a}, F. H. Liu³⁵, Fang Liu¹, Feng Liu⁶, H. B. Liu¹², H. H. Liu¹, H. H. Liu¹⁶, H. M. Liu¹, J. Liu¹, J. B. Liu^{46,a}, J. P. Liu⁵¹, J. Y. Liu¹, K. Liu³⁹, K. Y. Liu²⁷, L. D. Liu³¹, P. L. Liu^{1,a}, Q. Liu⁴¹, S. B. Liu^{46,a}, X. Liu²⁶, Y. B. Liu³⁰, Y. Y. Liu³⁰, Z. A. Liu^{1,a}, Zhiqing Liu²², H. Loehner²⁵, Y. F. Long³¹, X. C. Lou^{1,a,g}, H. J. Lu¹⁷, J. G. Lu^{1,a}, Y. Lu¹, Y. P. Lu^{1,a}, C. L. Luo²⁸, M. X. Luo⁵², T. Luo⁴², X. L. Luo^{1,a}, X. R. Lyu⁴¹, F. C. Ma²⁷, H. L. Ma¹, L. L. Ma³³, M. M. Ma¹, Q. M. Ma¹, T. Ma¹, X. N. Ma³⁰, X. Y. Ma^{1,a}, Y. M. Ma³³, F. E. Maas¹⁴, M. Maggiora^{49A,49C}, Q. A. Malik⁴⁸, Y. J. Mao³¹, Z. P. Mao¹, S. Marcello^{49A,49C}, J. G. Messchendorp²⁵, G. Mezzadri^{21B}, J. Min^{1,a}, T. J. Min¹, R. E. Mitchell¹⁹, X. H. Mo^{1,a}, Y. J. Mo⁶, C. Morales Morales¹⁴, G. Morello^{20A}, N. Yu. Muchnoi^{9,e}, H. Muramatsu⁴³, P. Musiol⁴, Y. Nefedov²³, F. Nerling¹⁰, I. B. Nikolaev^{9,e}, Z. Ning^{1,a}, S. Nisar⁸, S. L. Niu^{1,a}, X. Y. Niu¹, S. L. Olsen³², Q. Ouyang^{1,a}, S. Pacetti^{20B}, Y. Pan^{46,a}, P. Patteri^{20A}, M. Pelizaeus⁴, H. P. Peng^{46,a}, K. Peters^{10,i}, J. Pettersson⁵⁰, J. L. Ping²⁸, R. G. Ping¹, R. Poling⁴³, V. Prasad¹, H. R. Qi², M. Qi²⁹, S. Qian^{1,a}, C. F. Qiao⁴¹, L. Q. Qin³³, N. Qin⁵¹, X. S. Qin¹, Z. H. Qin^{1,a}, J. F. Qiu¹, K. H. Rashid⁴⁸, C. F. Redmer²², M. Ripka²², G. Rong¹, Ch. Rosner¹⁴, X. D. Ruan¹², A. Sarantsev^{23,f}, M. Savrié^{21B}, C. Schnier⁴, K. Schoenning⁵⁰, W. Shan³¹, M. Shao^{46,a}, C. P. Shen², P. X. Shen³⁰, X. Y. Shen¹, H. Y. Sheng¹, W. M. Song¹, X. Y. Song¹, S. Sosio^{49A,49C}, S. Spataro^{49A,49C}, G. X. Sun¹, J. F. Sun¹⁵, S. S. Sun¹, X. H. Sun¹, Y. J. Sun^{46,a}, Y. Z. Sun¹, Z. J. Sun^{1,a}, Z. T. Sun¹⁹, C. J. Tang³⁶, X. Tang¹, I. Tapan^{40C}, E. H. Thorndike⁴⁴, M. Tiemens²⁵, I. Uman^{40D}, G. S. Varner⁴², B. Wang³⁰, B. L. Wang⁴¹, D. Wang³¹, D. Y. Wang³¹, K. Wang^{1,a}, L. L. Wang¹, L. S. Wang¹, M. Wang³³, P. Wang¹, P. L. Wang¹, W. Wang^{1,a}, W. P. Wang^{46,a}, X. F. Wang³⁹, Y. Wang³⁷, Y. D. Wang¹⁴, Y. F. Wang^{1,a}, Y. Q. Wang²², Z. Wang^{1,a}, Z. G. Wang^{1,a}, Z. H. Wang^{46,a}, Z. Y. Wang¹, Z. Y. Wang¹, T. Weber²², D. H. Wei¹¹, P. Weidenkaff²², S. P. Wen¹, U. Wiedner⁴, M. Wolke⁵⁰, L. H. Wu¹, L. J. Wu¹, Z. Wu^{1,a}, L. Xia^{46,a}, L. G. Xia³⁹, Y. Xia¹⁸, D. Xiao¹, H. Xiao⁴⁷, Z. J. Xiao²⁸, Y. G. Xie^{1,a}, Y. H. Xie⁶, Q. L. Xiu^{1,a}, G. F. Xu¹, J. J. Xu¹, L. Xu¹, Q. J. Xu¹³, Q. N. Xu⁴¹, X. P. Xu³⁷, L. Yan^{49A,49C}, W. B. Yan^{46,a}, W. C. Yan^{46,a}, Y. H. Yan¹⁸, H. J. Yang^{34,j}, H. X. Yang¹, L. Yang⁵¹, Y. X. Yang¹¹, M. Ye^{1,a}, M. H. Ye⁷, J. H. Yin¹, Z. Y. You³⁸, B. X. Yu^{1,a}, C. X. Yu³⁰, J. S. Yu²⁶, C. Z. Yuan¹, Y. Yuan¹, A. Yuncu^{40B,b}, A. A. Zafar⁴⁸, Y. Zeng¹⁸, Z. Zeng^{46,a}, B. X. Zhang¹, B. Y. Zhang^{1,a}, C. C. Zhang¹, D. H. Zhang¹, H. H. Zhang³⁸, H. Y. Zhang^{1,a}, J. Zhang¹, J. J. Zhang¹, J. L. Zhang¹, J. Q. Zhang¹, J. W. Zhang^{1,a}, J. Y. Zhang¹, J. Z. Zhang¹, K. Zhang¹, L. Zhang¹, S. Q. Zhang³⁰, X. Y. Zhang³³, Y. Zhang¹, Y. Zhang¹, Y. H. Zhang^{1,a}, Y. N. Zhang⁴¹, Y. T. Zhang^{46,a}, Yu Zhang⁴¹, Z. H. Zhang⁶, Z. P. Zhang⁴⁶, Z. Y. Zhang⁵¹, G. Zhao¹, J. W. Zhao^{1,a}, J. Y. Zhao¹, J. Z. Zhao^{1,a}, Lei Zhao^{46,a}, Ling Zhao¹, M. G. Zhao³⁰, Q. Zhao¹, Q. W. Zhao¹, S. J. Zhao⁵³, T. C. Zhao¹, Y. B. Zhao^{1,a}, Z. G. Zhao^{46,a}, A. Zhemchugov^{23,c}, B. Zheng^{14,47}

J. P. Zheng^{1,a}, W. J. Zheng³³, Y. H. Zheng⁴¹, B. Zhong²⁸, L. Zhou^{1,a}, X. Zhou⁵¹, X. K. Zhou^{46,a}, X. R. Zhou^{46,a},
X. Y. Zhou¹, K. Zhu¹, K. J. Zhu^{1,a}, S. Zhu¹, S. H. Zhu⁴⁵, X. L. Zhu³⁹, Y. C. Zhu^{46,a}, Y. S. Zhu¹, Z. A. Zhu¹,
J. Zhuang^{1,a}, L. Zotti^{49A,49C}, B. S. Zou¹, J. H. Zou¹

(BESIII Collaboration)

- ¹ Institute of High Energy Physics, Beijing 100049, People's Republic of China
² Beihang University, Beijing 100191, People's Republic of China
³ Beijing Institute of Petrochemical Technology, Beijing 102617, People's Republic of China
⁴ Bochum Ruhr-University, D-44780 Bochum, Germany
⁵ Carnegie Mellon University, Pittsburgh, Pennsylvania 15213, USA
⁶ Central China Normal University, Wuhan 430079, People's Republic of China
⁷ China Center of Advanced Science and Technology, Beijing 100190, People's Republic of China
⁸ COMSATS Institute of Information Technology, Lahore, Defence Road, Off Raiwind Road, 54000 Lahore, Pakistan
⁹ G.I. Budker Institute of Nuclear Physics SB RAS (BINP), Novosibirsk 630090, Russia
¹⁰ GSI Helmholtzcentre for Heavy Ion Research GmbH, D-64291 Darmstadt, Germany
¹¹ Guangxi Normal University, Guilin 541004, People's Republic of China
¹² Guangxi University, Nanning 530004, People's Republic of China
¹³ Hangzhou Normal University, Hangzhou 310036, People's Republic of China
¹⁴ Helmholtz Institute Mainz, Johann-Joachim-Becher-Weg 45, D-55099 Mainz, Germany
¹⁵ Henan Normal University, Xinxiang 453007, People's Republic of China
¹⁶ Henan University of Science and Technology, Luoyang 471003, People's Republic of China
¹⁷ Huangshan College, Huangshan 245000, People's Republic of China
¹⁸ Hunan University, Changsha 410082, People's Republic of China
¹⁹ Indiana University, Bloomington, Indiana 47405, USA
²⁰ (A)INFN Laboratori Nazionali di Frascati, I-00044, Frascati, Italy; (B)INFN and University of Perugia, I-06100, Perugia, Italy
²¹ (A)INFN Sezione di Ferrara, I-44122, Ferrara, Italy; (B)University of Ferrara, I-44122, Ferrara, Italy
²² Johannes Gutenberg University of Mainz, Johann-Joachim-Becher-Weg 45, D-55099 Mainz, Germany
²³ Joint Institute for Nuclear Research, 141980 Dubna, Moscow region, Russia
²⁴ Justus-Liebig-Universitaet Giessen, II. Physikalisches Institut, Heinrich-Buff-Ring 16, D-35392 Giessen, Germany
²⁵ KVI-CART, University of Groningen, NL-9747 AA Groningen, The Netherlands
²⁶ Lanzhou University, Lanzhou 730000, People's Republic of China
²⁷ Liaoning University, Shenyang 110036, People's Republic of China
²⁸ Nanjing Normal University, Nanjing 210023, People's Republic of China
²⁹ Nanjing University, Nanjing 210093, People's Republic of China
³⁰ Nankai University, Tianjin 300071, People's Republic of China
³¹ Peking University, Beijing 100871, People's Republic of China
³² Seoul National University, Seoul, 151-747 Korea
³³ Shandong University, Jinan 250100, People's Republic of China
³⁴ Shanghai Jiao Tong University, Shanghai 200240, People's Republic of China
³⁵ Shanxi University, Taiyuan 030006, People's Republic of China
³⁶ Sichuan University, Chengdu 610064, People's Republic of China
³⁷ Soochow University, Suzhou 215006, People's Republic of China
³⁸ Sun Yat-Sen University, Guangzhou 510275, People's Republic of China
³⁹ Tsinghua University, Beijing 100084, People's Republic of China
⁴⁰ (A)Ankara University, 06100 Tandogan, Ankara, Turkey; (B)Istanbul Bilgi University, 34060 Eyup, Istanbul, Turkey; (C)Uludag University, 16059 Bursa, Turkey; (D)Near East University, Nicosia, North Cyprus, Mersin 10, Turkey
⁴¹ University of Chinese Academy of Sciences, Beijing 100049, People's Republic of China
⁴² University of Hawaii, Honolulu, Hawaii 96822, USA
⁴³ University of Minnesota, Minneapolis, Minnesota 55455, USA
⁴⁴ University of Rochester, Rochester, New York 14627, USA

⁴⁵ University of Science and Technology Liaoning, Anshan 114051, People's Republic of China

⁴⁶ University of Science and Technology of China, Hefei 230026, People's Republic of China

⁴⁷ University of South China, Hengyang 421001, People's Republic of China

⁴⁸ University of the Punjab, Lahore-54590, Pakistan

⁴⁹ (A)University of Turin, I-10125, Turin, Italy; (B)University of Eastern Piedmont, I-15121, Alessandria, Italy; (C)INFN, I-10125, Turin, Italy

⁵⁰ Uppsala University, Box 516, SE-75120 Uppsala, Sweden

⁵¹ Wuhan University, Wuhan 430072, People's Republic of China

⁵² Zhejiang University, Hangzhou 310027, People's Republic of China

⁵³ Zhengzhou University, Zhengzhou 450001, People's Republic of China

^a Also at State Key Laboratory of Particle Detection and Electronics, Beijing 100049, Hefei 230026, People's Republic of China

^b Also at Bogazici University, 34342 Istanbul, Turkey

^c Also at the Moscow Institute of Physics and Technology, Moscow 141700, Russia

^d Also at the Functional Electronics Laboratory, Tomsk State University, Tomsk, 634050, Russia

^e Also at the Novosibirsk State University, Novosibirsk, 630090, Russia

^f Also at the NRC "Kurchatov Institute", PNPI, 188300, Gatchina, Russia

^g Also at University of Texas at Dallas, Richardson, Texas 75083, USA

^h Also at Istanbul Arel University, 34295 Istanbul, Turkey

ⁱ Also at Goethe University Frankfurt, 60323 Frankfurt am Main, Germany

^j Also at Key Laboratory for Particle Physics, Astrophysics and Cosmology, Ministry of Education; Shanghai Key Laboratory for Particle Physics and Cosmology; Institute of Nuclear and Particle Physics, Shanghai 200240, People's Republic of China

Abstract

We study the decays of J/ψ and $\psi(3686)$ to the final states $\Sigma(1385)^0\bar{\Sigma}(1385)^0$ and $\Xi^0\bar{\Xi}^0$ based on a single baryon tag method using data samples of $(1310.6 \pm 7.0) \times 10^6$ J/ψ and $(447.9 \pm 2.9) \times 10^6$ $\psi(3686)$ events collected with the BESIII detector at the BEPCII collider. The decays to $\Sigma(1385)^0\bar{\Sigma}(1385)^0$ are observed for the first time. The measured branching fractions of J/ψ and $\psi(3686)$ to $\Xi^0\bar{\Xi}^0$ are in good agreement with, and much more precise than, the previously published results. The angular parameters for these decays are also measured for the first time. The measured angular decay parameter for $J/\psi \rightarrow \Sigma(1385)^0\bar{\Sigma}(1385)^0$, $\alpha = -0.64 \pm 0.03 \pm 0.10$, is found to be negative, different to the other decay processes in this measurement. In addition, the "12% rule" and isospin symmetry in the decays of J/ψ and $\psi(3686)$ to $\Xi\bar{\Xi}$ and $\Sigma(1385)\bar{\Sigma}(1385)$ are tested.

Keywords: charmonium, branching fraction, angular distribution

PACS: 12.38.Qk, 13.25.Gv

1. Introduction

The decays of the charmonium resonances J/ψ and $\psi(3686)$ [in the following, ψ denotes both charmonium states J/ψ and $\psi(3686)$] into baryon anti-baryon pairs ($B\bar{B}$) in e^+e^- annihilation have been extensively studied as a favorable test of perturbative quantum chromodynamics (QCD) [1]. These decays are assumed to proceed via the annihilation of the constituent $c\bar{c}$ pair into

three gluons or a virtual photon.

It is interesting that the $\psi(3686)$ decay to a specific final state is strongly suppressed relative to the same final state in J/ψ decay according to the annihilation decay of heavy quarkonium. The ratio of branching fractions for ψ decaying into the same final states is predicted from factorization [2] to be $\frac{B(\psi(3686) \rightarrow X)}{B(J/\psi \rightarrow X)} \approx 12\%$, where X denotes any exclusive hadronic decay

mode or the $\ell^+\ell^-$ ($\ell = e, \mu$) final state. This expectation is usually called the “12% rule”. This rule was first observed to be violated in the decay of ψ into the final state $\rho\pi$. A broad variety of reviews of the relevant theoretical and experimental results [3] conclude that the current theoretical explanations are unsatisfactory. Although the branching fractions for ψ decays into baryon pairs have been measured extensively [4], uncertainties are still large for many decays; *e.g.* the world average values of the branching fractions for J/ψ and $\psi(3686) \rightarrow \Xi^0\bar{\Xi}^0$ are $(1.20 \pm 0.24) \times 10^{-3}$ and $(2.07 \pm 0.23) \times 10^{-4}$ [4], respectively. In particular, $\psi \rightarrow \Sigma(1385)^0\bar{\Sigma}(1385)^0$ has not yet been observed.

By hadron helicity conservation, the angular distribution of the process $e^+e^- \rightarrow \psi \rightarrow B\bar{B}$ is expressed as

$$\frac{dN}{d\cos\theta} \propto 1 + \alpha \cos^2\theta, \quad (1)$$

where θ is the angle between the baryon and the beam directions in the e^+e^- center-of-mass (CM) system and α is a constant, which has widely been investigated in theory and experiment [5]. Theoretically, the value of α is discussed in the framework of many models, such as quark mass effects [6], or electromagnetic effects [7], which generally predict $0 < \alpha < 1$. BES measured the angular distribution of $J/\psi \rightarrow \Sigma^0\bar{\Sigma}^0$ and obtained a negative α with poor precision [8]. H. Chen *et al.* [9] explained that the angular distribution for $\psi \rightarrow B\bar{B}$ could be negative when rescattering effects of baryon and anti-baryon in heavy quarkonium decays are taken into consideration. Thus, experimental measurements of α are helpful to test the helicity conservation rule and the validity of the various theoretical approaches. In previous experiments, the angular distributions for charmonium decays to baryon pairs, such as $\psi \rightarrow p\bar{p}, \Lambda\bar{\Lambda}, \Sigma^0\bar{\Sigma}^0, \Xi^-\bar{\Xi}^+$, and $\Sigma(1385)^\mp\bar{\Sigma}(1385)^\pm$ [10, 11, 12, 13], were measured. However, angular distributions for the decays $\psi \rightarrow \Sigma(1385)^0\bar{\Sigma}(1385)^0$ and $\Xi^0\bar{\Xi}^0$ have not yet been measured.

In this Letter, we report the most precise measurements of the branching fractions and angular distributions for $\psi \rightarrow \Sigma(1385)^0\bar{\Sigma}(1385)^0$ and $\Xi^0\bar{\Xi}^0$ based on the data samples of $(1310.6 \pm 7.0) \times 10^6$ J/ψ [14] and $(447.9 \pm 2.9) \times 10^6$ $\psi(3686)$ [15, 16] events collected with the BESIII detector at BEPCII.

2. BESIII detector and Monte Carlo simulation

BEPCII is a double-ring e^+e^- collider that has reached a peak luminosity of $10^{33} \text{ cm}^{-2}\text{s}^{-1}$ at a CM energy of 3.773 GeV. The cylindrical core of the BESIII

detector consists of a helium-based main drift chamber (MDC), a plastic scintillator time-of-flight (TOF) system, and a CsI(Tl) electromagnetic calorimeter (EMC), which are all enclosed in a superconducting solenoidal magnet with a field strength of 1.0 T for the $\psi(3686)$ data and J/ψ data taken in 2009, and 0.9 T for the J/ψ data taken in 2012. The solenoid is supported by an octagonal flux-return yoke with resistive plate counter modules interleaved with steel as muon identifier. The acceptance for charged particles and photons is 93% of the 4π stereo angle, and the charged-particle momentum resolution at 1 GeV/ c is 0.5%. The photon energy resolution is 2.5% (5%) at 1.0 GeV in the barrel region (end caps regions). More details about the experimental apparatus can be found in Ref. [17].

The response of the BESIII detector is modeled with Monte Carlo (MC) simulations using a framework based on GEANT4 [18]. The production of ψ resonances is simulated with the KKMC generator [19], the subsequent decays are processed via EVTGEN [20] according to the measured branching fractions provided by the Particle Data Group (PDG) [4], and the remaining unmeasured decay modes are generated with LUNDCHARM [21]. To determine the detection efficiencies for $\psi \rightarrow \Sigma(1385)^0\bar{\Sigma}(1385)^0$ and $\Xi^0\bar{\Xi}^0$, one million MC events are generated for each mode taking into account for the angular distribution with α value measured in this analysis. The decays of the baryons $\Sigma(1385)^0$, Ξ^0 , and Λ in the signal channels are simulated exclusively, taking into account the angular distributions via EVTGEN [20], while the anti-baryons are set to decay inclusively.

3. Event selection

The selection of $\psi \rightarrow \Sigma(1385)^0\bar{\Sigma}(1385)^0$ and $\Xi^0\bar{\Xi}^0$ events via a full reconstruction of both $\Sigma(1385)^0/\Xi^0$ and $\bar{\Sigma}(1385)^0/\bar{\Xi}^0$ suffers from low reconstruction efficiency and large systematic uncertainty.

To achieve higher efficiency and reduce the systematic uncertainty, a single baryon $\Sigma(1385)^0/\Xi^0$ tag technique is employed, without including the anti-baryon mode tag due to the imperfection of the simulation related to the effect of annihilation for anti-proton. The $\Sigma(1385)^0/\Xi^0$ is reconstructed in its decay to $\pi^0\Lambda$ with the subsequent decays $\Lambda \rightarrow p\pi^-$ and $\pi^0 \rightarrow \gamma\gamma$. The charged tracks are required to be reconstructed in the MDC with good helix fits and within the angular coverage of the MDC ($|\cos\theta| < 0.93$, where θ is the polar angle with respect to the e^+ beam direction). Information from the specific energy loss measured in the MDC

(dE/dx) and from the TOF are combined to form particle identification (PID) confidence levels for the hypotheses of a pion, kaon, and proton. Each track is assigned to the particle type with the highest confidence level. At least one negatively charged pion and one proton are required. Photons are reconstructed from isolated showers in the EMC. The energy deposited in the nearby TOF counter is included to improve the reconstruction efficiency and energy resolution. Photon energies are required to be greater than 25 MeV in the EMC barrel region ($|\cos\theta| < 0.8$) or greater than 50 MeV in the EMC end cap ($0.86 < |\cos\theta| < 0.92$). The showers in the angular range between the barrel and the end cap are poorly reconstructed and are excluded from the analysis. Furthermore, the EMC timing of the photon candidate must be in coincidence with collision events, $0 \leq t \leq 700$ ns, to suppress electronic noise and energy deposits unrelated to the collision events. At least two good photon candidates are required.

In order to reconstruct the π^0 candidates, a one-constraint (1C) kinematic fit is employed for all $\gamma\gamma$ combinations, constraining the invariant mass of two photons to the π^0 nominal mass, combined with the requirement of $|\Delta E|/P_{\pi^0} < 0.95$, where ΔE is the energy difference between the two photons and P_{π^0} is the π^0 momentum, and the $\chi^2_{1C} < 20$ to suppress non- π^0 backgrounds.

To reconstruct the Λ candidates, a vertex fit is applied to all $p\pi^-$ combinations; the ones characterized by $\chi^2 < 500$ are kept for further analysis. The $p\pi$ invariant mass is required to be within 5 MeV/c^2 of the nominal Λ mass, determined by optimizing the figure of merit $\text{FOM} = \frac{S}{\sqrt{S+B}}$, where S is the number of signal events and B is the number of background events based on the MC simulation. To further suppress the background, the decay length of Λ is required to be larger than zero. The $\Sigma(1385)^0/\Xi^0$ candidates are reconstructed with Λ and π^0 candidates by minimizing the variable $|M_{\pi^0\Lambda} - M_{\Sigma(1385)^0/\Xi^0}|$, where $M_{\pi^0\Lambda}$ is the invariant mass of the $\pi^0\Lambda$ pair, and $M_{\Sigma(1385)^0/\Xi^0}$ is the nominal mass of $\Sigma(1385)^0/\Xi^0$.

The anti-baryon candidate $\bar{\Sigma}(1385)^0/\bar{\Xi}^0$ is inferred by the mass recoiling against the selected $\pi^0\Lambda$ system,

$$M_{\pi^0\Lambda}^{\text{recoil}} = \sqrt{(E_{\text{CM}} - E_{\pi^0\Lambda})^2 - \vec{p}_{\pi^0\Lambda}^2}, \quad (2)$$

where $E_{\pi^0\Lambda}$ and $\vec{p}_{\pi^0\Lambda}$ are the energy and momentum of the selected $\pi^0\Lambda$ system, and E_{CM} is CM energy. Figure 1 shows the scatter plot of $M_{\pi^0\Lambda}$ versus $M_{\pi^0\Lambda}^{\text{recoil}}$. Clear accumulations of events corresponding to the signals of $\psi \rightarrow \Sigma(1385)^0\bar{\Sigma}(1385)^0$ and $\Xi^0\bar{\Xi}^0$ decays are observed. The distributions of $M_{\pi^0\Lambda}$ with the additional

requirement of the $M_{\pi^0\Lambda}^{\text{recoil}}$ within $\pm 80 \text{ MeV}/c^2$ around $M_{\Sigma(1385)^0}$ or $\pm 50 \text{ MeV}/c^2$ around M_{Ξ^0} are shown in Fig. 2. Clear $\Sigma(1385)^0/\bar{\Xi}^0$ signals are observed.

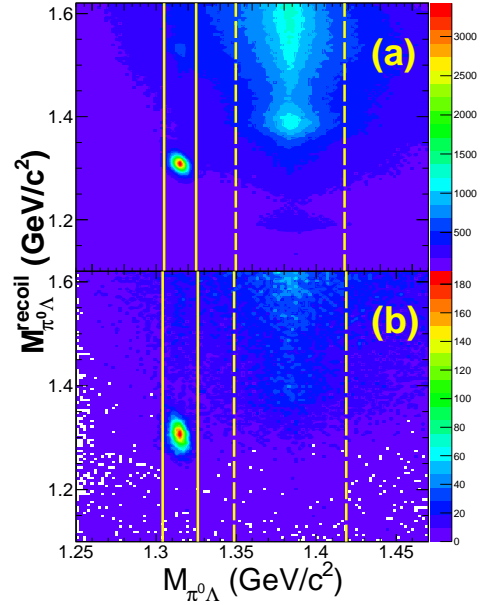


FIG. 1: Scatter plots of $M_{\pi^0\Lambda}$ versus $M_{\pi^0\Lambda}^{\text{recoil}}$ for (a) J/ψ and (b) $\psi(3686)$ data. The dashed lines denote the $\Sigma(1385)^0$ signal region, and the solid lines denote the Ξ^0 signal region.

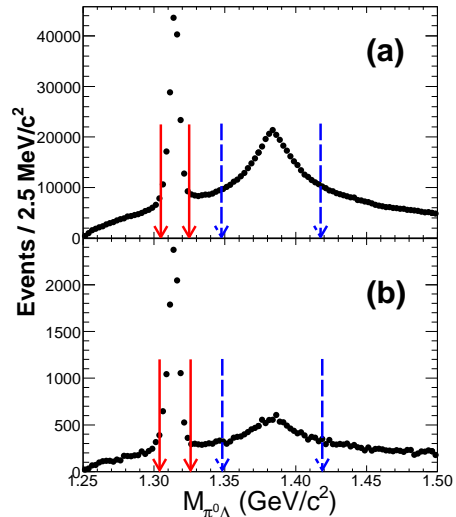


FIG. 2: Distribution of $M_{\pi^0\Lambda}$ for (a) J/ψ and (b) $\psi(3686)$ data. The arrows denote the applied requirements, where the dashed arrows show the $\Sigma(1385)^0$ signal region and the solid arrows show the Ξ^0 signal region.

To determine signal yields, the mass of $\pi^0\Lambda$ is required to be within $\pm 34 \text{ MeV}/c^2$ for $J/\psi \rightarrow$

$\Sigma(1385)^0\bar{\Sigma}(1385)^0$, $\pm 10 \text{ MeV}/c^2$ for $J/\psi \rightarrow \Xi^0\bar{\Xi}^0$, $\pm 35 \text{ MeV}/c^2$ for $\psi(3686) \rightarrow \Sigma(1385)^0\bar{\Sigma}(1385)^0$, and $\pm 11 \text{ MeV}/c^2$ for $\psi(3686) \rightarrow \Xi^0\bar{\Xi}^0$, around the nominal mass of $\Sigma(1385)^0/\bar{\Xi}^0$; the requirements are optimized by the FOM. For the $\psi(3686)$ decays, the requirements of $|M_{\pi^+\pi^-}^{\text{recoil}} - M_{J/\psi}| > 0.005 \text{ GeV}/c^2$ and $|M_{\pi^0\pi^0}^{\text{recoil}} - M_{J/\psi}| > 0.015 \text{ GeV}/c^2$ are used to suppress the backgrounds $\psi(3686) \rightarrow \pi\pi J/\psi$, where $M_{\pi^+\pi^-}^{\text{recoil}}$ and $M_{\pi^0\pi^0}^{\text{recoil}}$ are the recoil masses of any $\pi^+\pi^-$ and $\pi^0\pi^0$ combination if found, and $M_{J/\psi}$ is the J/ψ nominal mass according to the PDG [4].

4. Background study

The data collected at CM energies of 3.08 GeV (30 pb^{-1}) [14] and 3.65 GeV (44 pb^{-1}) [16] are used to estimate the contributions from the continuum processes $e^+e^- \rightarrow \Sigma(1385)^0\bar{\Sigma}(1385)^0$ and $\Xi^0\bar{\Xi}^0$. By applying the same event selection criteria, only a few events survive and do not form any obvious peaking structures in the $\bar{\Sigma}(1385)^0/\bar{\Xi}^0$ signal regions in the corresponding $M_{\pi^0\Lambda}^{\text{recoil}}$ distributions. Taking into account the normalization of the luminosity and CM energy dependence of the cross section, the QED backgrounds are found to be negligible.

The contamination from other background sources is analyzed using samples of MC simulated events of generic ψ decays that contain the same number of events as the data. After applying the same event selection, it is found that the peaking backgrounds for the $\psi \rightarrow \Sigma(1385)^0\bar{\Sigma}(1385)^0$ mode mainly come from $\psi \rightarrow \Xi^0\bar{\Xi}^0$, $\Xi^-\bar{\Xi}^+$, $\Sigma(1385)^-\bar{\Sigma}(1385)^+$, $\Xi(1530)\bar{\Xi} + \text{c.c.}$, and $\pi^0\Lambda\bar{\Sigma}(1385)^0$, where the branching fractions for $\psi \rightarrow \Xi(1530)\bar{\Xi} + \text{c.c.}$ and $\pi^0\Lambda\bar{\Sigma}(1385)^0$ are taken from the isospin partner modes $J/\psi \rightarrow \Xi(1530)\bar{\Xi} + \text{c.c.}$ [4] and $\pi^-\Lambda\bar{\Sigma}(1385)^+$ [13] based on the assumption of 12% rule. For the $J/\psi \rightarrow \Xi^0\bar{\Xi}^0$ mode, the peaking backgrounds are found to be from $J/\psi \rightarrow \Xi^-\bar{\Xi}^+$, $\gamma\eta_c(\gamma\Sigma^0\bar{\Sigma}^0, \gamma\Xi^0\bar{\Xi}^0)$, $\Sigma^0\bar{\Sigma}(1385)^0$, and $\Sigma^0\bar{\Sigma}^0$. For the $\psi(3686) \rightarrow \Xi^0\bar{\Xi}^0$ mode, the peaking background is from $\psi(3686) \rightarrow \Sigma^0\bar{\Sigma}^0$, and other backgrounds are found to be distributed smoothly in $M_{\pi^0\Lambda}^{\text{recoil}}$ mass spectrum.

The final states of baryon and anti-baryon decays both include a neutral pion with almost the same momenta. The π^0 from the anti-baryon can be wrongly combined with the Λ in the $\Sigma(1385)^0/\bar{\Xi}^0$ reconstruction. As a result, the wrong combination background (WCB) in the $\pi^0\Lambda$ mass spectrum is inevitable. This background is studied by the MC simulation.

5. Results

5.1. Branching fraction

The signal yields for the decays $\psi \rightarrow \Sigma(1385)^0\bar{\Sigma}(1385)^0$ and $\Xi^0\bar{\Xi}^0$ are extracted by performing an extended maximum likelihood fit to the $M_{\pi^0\Lambda}^{\text{recoil}}$ spectrum. In the fit, the signal shape is represented by the simulated MC shape convolved with a Gaussian function to take into account the mass resolution difference between data and MC simulation. The peaking backgrounds and the wrong combination background are described by the individual shape taken from MC simulation, and the corresponding numbers of background events are fixed according to the individual detection efficiencies and branching fractions [4]. The remaining backgrounds are found to be distributed smoothly in the $M_{\pi^0\Lambda}^{\text{recoil}}$ spectrum and are therefore described by a second-order polynomial function. Figure 3 shows the projection plots of $M_{\pi^0\Lambda}^{\text{recoil}}$ for the decays $\psi \rightarrow \Sigma(1385)^0\bar{\Sigma}(1385)^0$ and $\Xi^0\bar{\Xi}^0$, respectively.

The branching fraction can be calculated by

$$\mathcal{B}[\psi \rightarrow X\bar{X}] = \frac{N_{\text{obs}}}{N_{\psi} \cdot \epsilon \cdot \mathcal{B}(X \rightarrow \pi^0\Lambda) \cdot \mathcal{B}(\Lambda \rightarrow p\pi) \cdot \mathcal{B}(\pi^0 \rightarrow \gamma\gamma)},$$

where X stands for the $\Sigma(1385)^0$ or Ξ^0 baryon, ϵ denotes the detection efficiency obtained with the measured α value, N_{obs} is the number of observed signal events, $\mathcal{B}(X \rightarrow \pi^0\Lambda)$, $\mathcal{B}(\Lambda \rightarrow p\pi)$ and $\mathcal{B}(\pi^0 \rightarrow \gamma\gamma)$ are the branching fractions of $X \rightarrow \Lambda\pi^0$, $\Lambda \rightarrow p\pi$ and $\pi^0 \rightarrow \gamma\gamma$ taken from PDG [4], N_{ψ} is the total number of J/ψ or $\psi(3686)$ events [14, 16]. Table 1 summarizes the numbers of observed signal events, the corresponding efficiencies, and branching fractions for the various decays in this measurement with the statistic uncertainty only.

5.2. Angular distribution

The values of α for the four decay processes are determined by performing a least squares fit to the $\cos\theta$ distribution in the range from -0.8 to 0.8 , divided into 8 equidistant intervals for the decays $\psi(3686) \rightarrow \Sigma(1385)^0\bar{\Sigma}(1385)^0$ and into 16 intervals for the other three decay modes.

The signal yield in each $\cos\theta$ bin is obtained with the aforementioned fit method. The distributions of the efficiency-corrected signal yields together with the fit curves are shown in Fig. 4. The α values obtained from the fits based on Eq. (1) are summarized in Table 1.

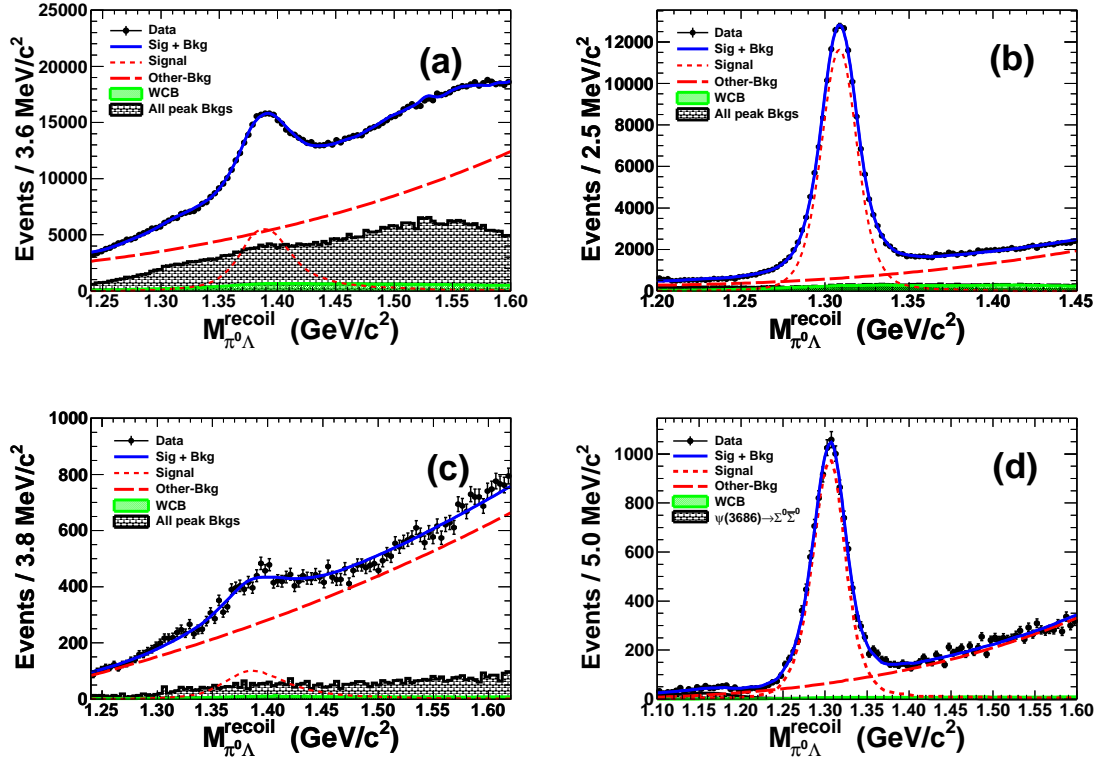


FIG. 3: (Color online). Recoil mass spectra of $\pi^0\Lambda$ for (a) $J/\psi \rightarrow \Sigma(1385)^0\bar{\Sigma}(1385)^0$, (b) $J/\psi \rightarrow \Xi^0\bar{\Xi}^0$, (c) $\psi(3686) \rightarrow \Sigma(1385)^0\bar{\Sigma}(1385)^0$, and (d) $\psi(3686) \rightarrow \Xi^0\bar{\Xi}^0$. Dots with error bars indicate the data, the blue solid lines show the fit result, the red short-dashed lines are for signal, the red long-dashed ones are for the remaining background (Other-Bkg), and the green hatched ones are for wrong combination background (WCB), the black hatched ones are for the peaking backgrounds.

TABLE I: The numbers of the observed events N_{obs} , efficiencies ϵ , α values, and branching fractions \mathcal{B} for $\psi \rightarrow \Sigma(1385)^0\bar{\Sigma}(1385)^0$ and $\Xi^0\bar{\Xi}^0$. Only the statistical uncertainties are indicated.

Channel	N_{obs}	$\epsilon(\%)$	α	$\mathcal{B}(\times 10^{-4})$
$J/\psi \rightarrow \Sigma(1385)^0\bar{\Sigma}(1385)^0$	102762 ± 852	13.32 ± 0.04	-0.64 ± 0.03	10.71 ± 0.09
$J/\psi \rightarrow \Xi^0\bar{\Xi}^0$	134846 ± 437	14.05 ± 0.04	0.66 ± 0.03	11.65 ± 0.04
$\psi(3686) \rightarrow \Sigma(1385)^0\bar{\Sigma}(1385)^0$	2214 ± 149	13.13 ± 0.03	0.59 ± 0.25	0.69 ± 0.05
$\psi(3686) \rightarrow \Xi^0\bar{\Xi}^0$	10839 ± 123	14.10 ± 0.04	0.65 ± 0.09	2.73 ± 0.03

6. Systematic uncertainty

6.1. Branching fraction

Systematic uncertainties on the branching fractions are mainly due to efficiency differences between data and MC simulation. They are estimated by comparing the efficiencies of photon, π^0 , Λ and Ξ^0 reconstruction between the data and the MC simulation. Additional sources of systematic uncertainties are the fit

range, wrong combination, the background shape, and the angular distributions. In addition, the uncertainties of the decay branching fractions of intermediate states and uncertainties of the total number of ψ events are also accounted for in the systematic uncertainty. All of the systematic uncertainties are discussed in detail below.

1. The uncertainty associated with photon detection efficiency is 1.0% per photon, which is de-

terminated using the control sample $J/\psi \rightarrow \rho\pi$. Hence, for $\psi \rightarrow \Sigma(1385)^0\bar{\Sigma}(1385)^0$, the value 2.0% is taken as the systematic uncertainty.

2. The systematic uncertainty due to the 1C kinematic fit for the π^0 reconstruction is estimated to be 1.0% with the control sample $J/\psi \rightarrow \rho\pi$.
3. The uncertainty related to the Λ reconstruction efficiency in $\Sigma(1385)$ decays is estimated using the control sample $\psi \rightarrow \Xi^-\bar{\Xi}^+$. Here, the Λ reconstruction efficiency includes systematic uncertainties due to tracking, PID, and the vertex fit. A detailed description of this method can be found in Ref. [22].

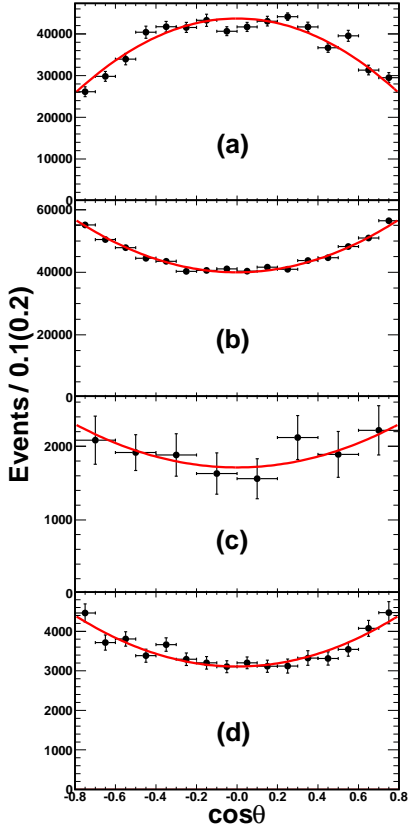


FIG. 4: Distributions of $\cos\theta$ for (a) $J/\psi \rightarrow \Sigma(1385)^0\bar{\Sigma}(1385)^0$, (b) $J/\psi \rightarrow \Xi^0\bar{\Xi}^0$, (c) $\psi(3686) \rightarrow \Sigma(1385)^0\bar{\Sigma}(1385)^0$, and (d) $\psi(3686) \rightarrow \Xi^0\bar{\Xi}^0$. The dots with error bars indicate the efficiency corrected data, and the curves show the fit results.

4. The Ξ^0 reconstruction efficiency, which includes the two photon efficiencies, π^0 reconstruction efficiency and the Λ reconstruction efficiency, is studied with the control sample $J/\psi \rightarrow \Xi^0\bar{\Xi}^0$ via single and double tag methods. The selection

criteria of the charged tracks, and the reconstruction of Λ and Ξ^0 candidates are exactly same as those described in Sec. 3. The Ξ^0 reconstruction efficiency is defined as the ratio of the number of events from the double tag $\Xi^0\bar{\Xi}^0$ to that from the single tag. The difference in the Ξ^0 reconstruction efficiency between data and MC samples is taken as the systematic uncertainty.

5. In the fits of the $M_{\pi^0\Lambda}^{\text{recoil}}$ signal, the uncertainty due to the fitting range is estimated by varying the mass range by $\pm 10 \text{ MeV}/c^2$ for two sides. The resulting differences of signal yields are taken as the systematic uncertainty.
6. The uncertainties due to the background shape arise from the polynomial function and the peaking shape. The former is estimated by the alternative fits with a first or a third-order polynomial function. The latter is estimated by varying the number of normalized events by 1σ . The larger difference is taken as the systematic uncertainty. The total uncertainty related to the background shape is obtained by adding all contributions in quadrature.
7. The systematic uncertainty due to the wrong combination background is estimated by comparing the signal yields between the fits with and without the corresponding component included in the fit. The differences of signal yields are taken as systematic uncertainties.
8. The uncertainty related with the detection efficiency due to the modeling of the angular distribution of the baryon pairs, represented by the parameter α , is estimated by varying the measured α values by 1σ in the MC simulation. The changes in the detection efficiency are taken as a systematic uncertainty.
9. The systematic uncertainties due to the branching fractions of the intermediate states, Ξ^0 , $\Sigma(1385)^0$ and Λ , are taken from the PDG [4]. They are 1.9% for $\psi \rightarrow \Sigma(1385)^0\bar{\Sigma}(1385)^0$ and 0.8% for $\psi \rightarrow \Xi^0\bar{\Xi}^0$.
10. The systematic uncertainties due to the total number of J/ψ or $\psi(3686)$ events are determined with the inclusive hadronic ψ decays. They are 0.5% and 0.6% in [14, 16], respectively.

The various systematic uncertainties on the branching fraction measurements are summarized in Table 2. The total systematic uncertainty is obtained by summing the individual contributions in quadrature.

TABLE 2: Relative systematic uncertainties on the branching fraction measurements (in %).

Source	$J/\psi \rightarrow$		$\psi(3686) \rightarrow$	
	$\Sigma(1385)^0 \bar{\Sigma}(1385)^0$	$\Xi^0 \bar{\Xi}^0$	$\Sigma(1385)^0 \bar{\Sigma}(1385)^0$	$\Xi^0 \bar{\Xi}^0$
Photon efficiency	2.0	...	2.0	...
π^0 reconstruction	1.0	...	1.0	...
Λ reconstruction	3.0	...	1.0	...
Ξ^0 reconstruction	...	2.6	...	2.6
Fit range	2.1	1.6	2.8	1.8
Background shape	3.9	1.5	4.0	2.3
Wrong combination	4.2	0.8	4.5	0.3
Angular distribution	2.0	0.5	1.2	2.8
Intermediate decay	1.9	0.8	1.9	0.8
Total number of ψ	0.5	0.5	0.6	0.6
Total	7.7	3.7	7.4	4.9

6.2. Angular distribution

Various systematic uncertainties are considered in the measurement of the values of α . These include the uncertainty of the signal yield in the different $\cos\theta$ intervals, the uncertainty of the $\cos\theta$ fit procedure, and the uncertainty related to the detection efficiency correction curve as function of the $\cos\theta$ bin. They are discussed in detail below.

1. The signal yields in each $\cos\theta$ interval are determined by the fit to the corresponding $M_{\pi^0\Lambda}^{\text{recoil}}$ distribution. The sources of the systematic uncertainty of the signal yield include the fit range, the background shape, MC resolution and wrong combination, where the MC resolution is fixed for the decay $\psi(3686) \rightarrow \Sigma(1385)^0 \bar{\Sigma}(1385)^0$ only. To estimate the systematic uncertainty related with fit range on $M_{\pi^0\Lambda}^{\text{recoil}}$, we repeat the fit to the $M_{\pi^0\Lambda}^{\text{recoil}}$ distribution by changing the fit range by $\pm 10 \text{ MeV}/c^2$. Then, the α values are extracted by the fit with the changed signal yield, and the resulting differences to the nominal α values are taken as the systematic uncertainties. The uncertainties related to the background shape, MC resolution and wrong combination backgrounds in the fit are evaluated with a method similar to the one described above.
2. The systematic uncertainties related to the procedure of the fit on the $\cos\theta$ distribution are estimated by re-fitting the $\cos\theta$ distribution with a different binning and fit range. We divide $\cos\theta$ into 8 intervals for $\psi \rightarrow \Xi^0 \bar{\Xi}^0$ and 16 intervals for $\psi \rightarrow \Sigma(1385)^0 \bar{\Sigma}(1385)^0$. The changes of the α values are taken as systematic uncertainties. We

also repeat the fit by changing the range to $[-0.9, 0.9]$ or $[-0.7, 0.7]$ in $\cos\theta$, with the same bin size of the nominal fit. The largest differences of α value with respect to the nominal value are taken as a systematic uncertainties.

3. In the analysis, the α values are obtained by fitting the $\cos\theta$ distribution corrected by the detection efficiency. To estimate the systematic uncertainty related to the imperfect simulation of the detection efficiency, the ratio of detection efficiencies as function of $\cos\theta$ between data and MC simulation is obtained based on the control sample $J/\psi \rightarrow \Xi^0 \bar{\Xi}^0$ with a full event reconstruction. Then, the efficiency corrected $\cos\theta$ distribution scaled by the ratios of detection efficiencies is re-fitted. The resulting differences in α are taken as the systematic uncertainty.

All the systematic uncertainties for the α measurement are summarized in Table 3. The total systematic uncertainty is the quadratic sum of the individual values.

7. Conclusion and discussion

Using $(1310.6 \pm 7.0) \times 10^6$ J/ψ and $(447.9 \pm 2.9) \times 10^6$ $\psi(3686)$ events collected with the BESIII detector at BEPCII, the branching fractions and the angular distributions for $\psi \rightarrow \Sigma(1385)^0 \bar{\Sigma}(1385)^0$ and $\Xi^0 \bar{\Xi}^0$ are measured. A comparison of the branching fractions between our measurement and previous experiments (PDG average) is summarized in Table 4. The branching fractions for $\psi \rightarrow \Sigma(1385)^0 \bar{\Sigma}(1385)^0$ are measured for the first time, and the branching fractions for $\psi \rightarrow \Xi^0 \bar{\Xi}^0$ are measured with a good agreement

TABLE 3: Relative systematic uncertainties on the α value measurements (in %).

Source	$J/\psi \rightarrow$		$\psi(3686) \rightarrow$	
	$\Sigma(1385)^0 \Sigma(1385)^0$	$\Xi^0 \Xi^0$	$\Sigma(1385)^0 \Sigma(1385)^0$	$\Xi^0 \Xi^0$
$M_{\pi^0 \Lambda}^{\text{recoil}}$ fitting range	7.8	3.0	15.3	7.7
Background shape	3.2	3.0	20.0	4.6
MC resolution	16.9	...
Wrong combination	4.7	1.5	5.1	15.0
$\cos \theta$ interval	7.8	3.5	22.0	10.4
$\cos \theta$ fitting range	7.8	3.0	15.6	3.5
Efficiency correction	4.7	3.0	9.0	3.0
Total	15.4	7.1	41.8	20.8

and a much higher precision than the previous results. The measured α values are also compared with the predictions of the theoretical models from Refs. [6, 7]. As indicated in Table 5, some of our results disagree significantly with the theoretical predictions, which may imply that the naive prediction of QCD suffers from the approximation that higher-order corrections are not taken into account. As calculated in Ref. [9], the sign for parameter α in $\psi \rightarrow \Sigma^0 \Sigma^0$ mode could be negative if re-scattering effects in the final states are taken into account. However, our results show that α for J/ψ is negative, and is different to the other decay processes in this measurement, which is hard to explain within the existing models. We, therefore, believe that it is of utmost importance to improve the theoretical models to shed further light on the origin of these discrepancies.

To test the “12% rule”, the ratios of the branching fractions $\frac{\mathcal{B}(\psi(3686) \rightarrow \Sigma(1385)^0 \Sigma(1385)^0)}{\mathcal{B}(J/\psi \rightarrow \Sigma(1385)^0 \Sigma(1385)^0)}$ and $\frac{\mathcal{B}(\psi(3686) \rightarrow \Xi^0 \Xi^0)}{\mathcal{B}(J/\psi \rightarrow \Xi^0 \Xi^0)}$ are calculated to be $(6.44 \pm 0.47 \pm 0.64)\%$ and $(23.43 \pm 0.26 \pm 1.09)\%$, respectively, taking into account the cancelation of the common systematic uncertainties. The ratios are not in agreement with 12%, especially for the $\Xi^0 \Xi^0$ final state.

To test isospin symmetry, the ratios of the branching fractions listed in Table 6 are also calculated based on the measurements between the neutral mode and the corresponding charged modes [13] taking into account the cancelation of the common systematic uncertainties. All ratios are within 1σ of the expectation of isospin symmetry.

8. Acknowledgement

The BESIII collaboration thanks the staff of BEPCII and the IHEP computing center for their strong support. This work is supported in part by National

Key Basic Research Program of China under Contract No. 2015CB856700; National Natural Science Foundation of China (NSFC) under Contracts Nos. 11235011, 11322544, 11335008, 11425524, 11475207, 11505034, 11565006, 11635010; the Chinese Academy of Sciences (CAS) Large-Scale Scientific Facility Program; the CAS Center for Excellence in Particle Physics (CCEPP); the Collaborative Innovation Center for Particles and Interactions (CICPI); Joint Large-Scale Scientific Facility Funds of the NSFC and CAS under Contracts Nos. U1232107, U1232201, U1332201, U1532257, U1532258; CAS under Contracts Nos. KJCX2-YW-N29, KJCX2-YW-N45; 100 Talents Program of CAS; National 1000 Talents Program of China; INPAC and Shanghai Key Laboratory for Particle Physics and Cosmology; German Research Foundation DFG under Contracts Nos. Collaborative Research Center CRC 1044, FOR 2359; Istituto Nazionale di Fisica Nucleare, Italy; Koninklijke Nederlandse Akademie van Wetenschappen (KNAW) under Contract No. 530-4CDP03; Ministry of Development of Turkey under Contract No. DPT2006K-120470; The Swedish Research Council; U. S. Department of Energy under Contracts Nos. DE-FG02-05ER41374, DE-SC-0010504, DE-SC-0010118, DE-SC-0012069; U.S. National Science Foundation; University of Groningen (RuG) and the Helmholtzzentrum fuer Schwerionenforschung GmbH (GSI), Darmstadt; WCU Program of National Research Foundation of Korea under Contract No. R32-2008-000-10155-0.

9. References

References

- [1] S. J. Brodsky and G. P. Lepage, Phys. Rev. D **24** (1981) 2848; J. Bolz and P. Kroll, Eur. Phys. J. C **2** (1998) 545; R. G. Ping, H. C. Chiang and B. S. Zou, Phys. Rev. D **66** (2002) 054020.

TABLE 4: Comparison of the branching fractions for $\psi \rightarrow \Sigma(1385)^0 \bar{\Sigma}(1385)^0$ and $\Xi^0 \bar{\Xi}^0$ (in units of 10^{-4}). The first uncertainties are statistical, and the second systematic.

Mode	$J/\psi \rightarrow \Sigma(1385)^0 \bar{\Sigma}(1385)^0$	$J/\psi \rightarrow \Xi^0 \bar{\Xi}^0$	$\psi(3686) \rightarrow \Sigma(1385)^0 \bar{\Sigma}(1385)^0$	$\psi(3686) \rightarrow \Xi^0 \bar{\Xi}^0$
This work	$10.71 \pm 0.09 \pm 0.82$	$11.65 \pm 0.04 \pm 0.43$	$0.69 \pm 0.05 \pm 0.05$	$2.73 \pm 0.03 \pm 0.13$
BESII [23]	...	$12.0 \pm 1.2 \pm 2.1$
CLEO [24]	$2.75 \pm 0.64 \pm 0.61$
Dobbs <i>et al.</i> [25]	$2.02 \pm 0.19 \pm 0.15$
PDG [4]	...	12.0 ± 2.4	...	2.07 ± 0.23

TABLE 5: Comparison of the α values for $\psi \rightarrow \Sigma(1385)^0 \bar{\Sigma}(1385)^0$ and $\Xi^0 \bar{\Xi}^0$, the first uncertainties are statistical and the second systematic.

Mode	$J/\psi \rightarrow \Sigma(1385)^0 \bar{\Sigma}(1385)^0$	$J/\psi \rightarrow \Xi^0 \bar{\Xi}^0$	$\psi(3686) \rightarrow \Sigma(1385)^0 \bar{\Sigma}(1385)^0$	$\psi(3686) \rightarrow \Xi^0 \bar{\Xi}^0$
This work	$-0.64 \pm 0.03 \pm 0.10$	$0.66 \pm 0.03 \pm 0.05$	$0.59 \pm 0.25 \pm 0.25$	$0.65 \pm 0.09 \pm 0.14$
Carimalo <i>et al.</i> [6]	0.11	0.16	0.28	0.33
Claudson [7]	0.19	0.28	0.46	0.53

TABLE 6: Summary of the ratios of branching fraction for testing isospin symmetry. The first uncertainties are the statistical, and the second systematic.

Mode	$\frac{\mathcal{B}(\psi \rightarrow \Xi^0 \bar{\Xi}^0)}{\mathcal{B}(\psi \rightarrow \Xi^- \bar{\Xi}^+)}$	$\frac{\mathcal{B}(\psi \rightarrow \Sigma(1385)^0 \bar{\Sigma}(1385)^0)}{\mathcal{B}(\psi \rightarrow \Sigma(1385)^- \bar{\Sigma}(1385)^+)}$	$\frac{\mathcal{B}(\psi \rightarrow \Sigma(1385)^0 \bar{\Sigma}(1385)^0)}{\mathcal{B}(\psi \rightarrow \Sigma(1385)^+ \bar{\Sigma}(1385)^-)}$
J/ψ	$1.12 \pm 0.01 \pm 0.07$	$0.98 \pm 0.01 \pm 0.08$	$0.85 \pm 0.02 \pm 0.09$
$\psi(3686)$	$0.98 \pm 0.02 \pm 0.07$	$0.81 \pm 0.12 \pm 0.12$	$0.82 \pm 0.11 \pm 0.11$

- [2] T. Appelquist and H. D. Politzer, Phys. Rev. Lett. **34** (1975) 43; D. M. Asner *et al.*, Int. J. Mod. Phys. A **24** (2009).
- [3] Y. F. Gu and X. H. Li, Phys. Rev. D **63** (2001) 114019; X. H. Mo, C. Z. Yuan and P. Wang, High Energy Physics and Nuclear Physics **31** (2007) 686; Quarkonium Working Group, N. Brambilla *et al.*, Eur. Phys. J. C **71** (2011) 1534; Q. Wang, G. Li, and Q. Zhao, Phys. Rev. D **85** (2012) 074015.
- [4] Particle Data Group, C. Patrignani *et al.*, Chin. Phys. C **40** (2016) 100001.
- [5] F. Murgia and M. Melis, Phys. Rev. D **51** (1995) 3487; BES Collaboration, J. Z. Bai, *et al.*, Phys. Lett. B **591** (2004) 42; BES Collaboration, M. Ablikim, *et al.*, Phys. Lett. B **632** (2006) 181; Fermilab E835 Collaboration, A. Buzzo, *et al.*, Phys. Lett. B **610** (2005) 177.
- [6] C. Carimalo, Int. J. Mod. Phys. A **2** (1987) 249.
- [7] M. Claudson, S. L. Glashow and M. B. Wise, Phys. Rev. D **25**(1982) 1345.
- [8] BES Collaboration, M. Ablikim *et al.*, Phys. Lett. B **632** (2006) 181.
- [9] H. Chen and R. G. Ping, Phys. Lett. B **644** (2007) 54.
- [10] BES Collaboration, J. Z. Bai *et al.*, Phys. Lett. B **591** (2004).
- [11] BES Collaboration, M. Ablikim *et al.*, Phys. Lett. B **648** (2007) 149.
- [12] BES Collaboration, M. Ablikim *et al.*, Chin. Phys. C **36** (2012) 1031.
- [13] BESIII Collaboration, M. Ablikim *et al.*, Phys. Rev. D **93** (2016) 072003.
- [14] BESIII Collaboration, M. Ablikim *et al.*, Chin. Phys. C **41** (2017) no.1, 013001.
- [15] BESIII Collaboration, M. Ablikim *et al.*, Chin. Phys. C **37** (2013) 063001.
- [16] With the same method (see Ref. [15] for more details), the preliminary number of the $\psi(3686)$ events taken in 2009 and 2012 determined to be 447.9×10^6 with an uncertainty of 0.6%.
- [17] BESIII Collaboration, M. Ablikim *et al.*, Nucl. Instrum. Meth. A **614** (2010) 345.
- [18] GEANT4 Collaboration, S. Agostinelli *et al.*, Nucl. Instrum. Meth. A **506** (2003) 250; J. Allison *et al.*, IEEE Trans. Nucl. Sci. **53** (2006) 270.
- [19] S. Jadach, B. F. L. Ward and Z. Was, Comput. Phys. Commun. **130** (2000) 260; S. Jadach, B. F. L. Ward and Z. Was, Phys. Rev. D **63** (2001) 113009.
- [20] R. G. Ping *et al.*, Chin. Phys. C **32** (2008) 599; D. J. Lange, Nucl. Instrum. Meth. A **462** (2001) 152.
- [21] J. C. Chen, G. S. Huang, X. R. Qi, D. H. Zhang and Y. S. Zhu, Phys. Rev. D **62** (2000) 034003.
- [22] BESIII Collaboration, M. Ablikim, *et al.*, Phys. Rev. D **87** (3) (2013) 032007.
- [23] BES Collaboration, M. Ablikim *et al.*, Phys. Rev. D **78** (2008) 092005.
- [24] CLEO Collaboration, T. K. Pedlar *et al.*, Phys. Rev. D **72** (2005) 051108.
- [25] S. Dobbs, A. Tomaradze, T. Xiao, K. K. Seth and G. Bonvicini, Phys. Lett. B **739** (2014) 90.